Nanoscale

PAPER

View Article Online
View Journal | View Issue

Cite this: *Nanoscale*, 2015, **7**, 1927

On-chip read-out of picomechanical motion under ambient conditions

Gino Putrino,*[a] Mariusz Martyniuk,[a] Adrian Keating,[b] Lorenzo Faraone[a] and John Dell[a]

Received 17th September 2014,
Accepted 12th December 2014

DOI: 10.1039/c4nr05419a

www.rsc.org/nanoscale

Monitoring the nanomechanical movement of suspended cantilever structures has found use in applications ranging from biological/chemical sensing to atomic force microscopy. Interrogating these sensors relies on the ability to accurately determine the sub-nanometre movements of the cantilever. Here we investigate a technique based on the combination of integrated silicon photonics and microelectromechanical systems (MEMS) to create an optically resonant microcavity and demonstrate its use for monitoring of the position of cantilevers on the picometer scale under ambient conditions with dynamic range extending over several microns. The technique is interferometric, and we show it to be sufficiently sensitive to measure both the first and second modes of cantilever Brownian motion. We anticipate that application of this technique will provide a physically robust, picometer precision, integrated cantilever movement read-out technology which can take cantilever sensors from laboratory controlled environments into real world conditions, allowing everyday applications.

1. Introduction

The application of nanomechanical cantilever based technologies to chemical and biological sensors offers exciting opportunities. In recent years, these technologies have been used to demonstrate mass sensing with zeptogram (10^{-21} g) sensitivity[1,2] Nanomechanical movements of cantilevers can be used to sense a wide range of biological and chemical species. Over the past decade, such sensors have been demonstrated to provide the sensitivity to detect cancers such as melanoma[3] or prostate cancer,[4] weigh biomolecules, single cells and single nanoparticles,[5,6] and a host of other sensing applications.[7–11] Cantilever chemical and biological sensors are formed by coating a cantilever with a functionalization layer which preferentially adsorbs only the chemical to be sensed. The cantilever structure is affected when the chemical is adsorbed by the functionalization layer, and a detection event occurs. Interrogating these sensors relies on the ability to accurately determine the nanomechanical movements of the cantilever[12–14] and is of critical importance for any cantilever position interrogation technology. However, this high precision, needs to be attained and integrated for real world conditions away from the controlled environment of a lab in order to enable the raft of applications benefiting from cantilever sensing.[12,15] In addition, it is desirable to have the ability to simultaneously measure the positions of individual cantilevers grouped in large arrays to improve sensing statistics and to simultaneously monitor for multiple chemicals. This also can provide extra cantilevers without functionalization for use as control structures, *e.g.* for differential sensing or thermal compensation. Techniques to monitor the position of a suspended cantilever beam are also of importance in the design of atomic force microscopes (AFMs).

Contemporary techniques for detecting cantilever motion or position include traditional AFM based techniques (such as a laser beam reflected from the cantilever tip to a distant quadrant photodetector[12]), electrical sensing (such as piezoresistive, piezoelectric, capacitive, Lorentz force/emf sensing and tunnelling current techniques), and optical sensing based on optical interference, or the use of diffraction from an optical grating formed by a line of cantilevers.[1,16,17]

Generally speaking, integrated electrical sensing techniques are capable of interrogating larger arrays of devices with lower sensitivity than optical techniques,[18] whilst optical techniques have higher sensitivity than electrical techniques but struggle to interrogate large cantilever arrays.[19] For the wider deployment of cantilever sensors to be achieved, it is necessary to keep the sensitivity of the best optical techniques, and gain the ability to address large (>20) arrays of cantilevers using a method that is compatible with ambient conditions, and which does not cause alignment and integration issues.[15] This is currently a very active and competitive area of research,

[a]*The University of Western Australia, School of Electrical, Electronic and Computer Engineering, University of Western Australia, Perth, WA 6009, Australia. E-mail: gino.putrino@uwa.edu.au*
[b]*The University of Western Australia, School of Mechanical and Chemical Engineering, University of Western Australia, Perth, WA 6009, Australia*

with novel techniques being recently reported that include using cantilevers as optical waveguides,[20] an optical differential detection method,[21] and a photonic microharp array technique.[22]

The work described herein focuses on an integrated on-chip resonant optical interferometric technique for monitoring of cantilevers with picometre-scale position accuracy. This technique has the potential to be easily integrated to read-out the deflections of individual cantilevers in large dense arrays[23] and can be fabricated using standard CMOS processes. We demonstrate the operation of the technique on electrically actuated cantilevers by confirming that characterisation of cantilever mechanical motion as measured using our approach, a commercial vibrometer and cantilever mechanical theory agree, and demonstrate picometre-scale measurement of cantilever position. Subsequently, we perform a multiple wavelength study to demonstrate the design's ability to operate over a broad range of optical wavelengths, and show that the technique is sufficiently sensitive to detect both the first and second modes of cantilever Brownian motion stimulated in ambient conditions. As such, this opens the doors to a number of biological and chemical sensing applications which until now have been limited to lab environments.

2. Device concept and mechanical operation

An isometric view of the cantilever and the read-out structure is shown in Fig. 1(a). A suspended cantilever is fabricated above a diffraction grating etched into a single mode silicon waveguide. When the mechanical cantilever beam is deflected, the gap between underside of the cantilever and the grating in the waveguide changes. If the underside of the cantilever is made reflective, then an optically resonant cavity will be created between the underside of the cantilever and the diffraction grating for light propagating through the waveguide as some of the waveguided light is diffracted by the interrogating grating out of the plane of the waveguide and towards the cantilever. The cantilever reflects the light back to the interrogating grating, where it interferometrically interacts with the non-diffracted waveguided light depending on the travelled path length. Effectively, the intensity of the light downstream of the cantilever is amplitude modulated by cantilever motion above the waveguide, providing an extremely sensitive measure of the cantilever deflection.

Cantilever sensors have two modes of operation: either static operation, where the change in cantilever deflection is measured, or dynamic operation, where the change in cantilever resonant frequency is measured.[24] The described design device concept is applicable to both operating modes.

3. Fabrication of device and experimental setup

The waveguides and diffraction gratings were first modelled using the MEEP finite difference time domain (FDTD) software

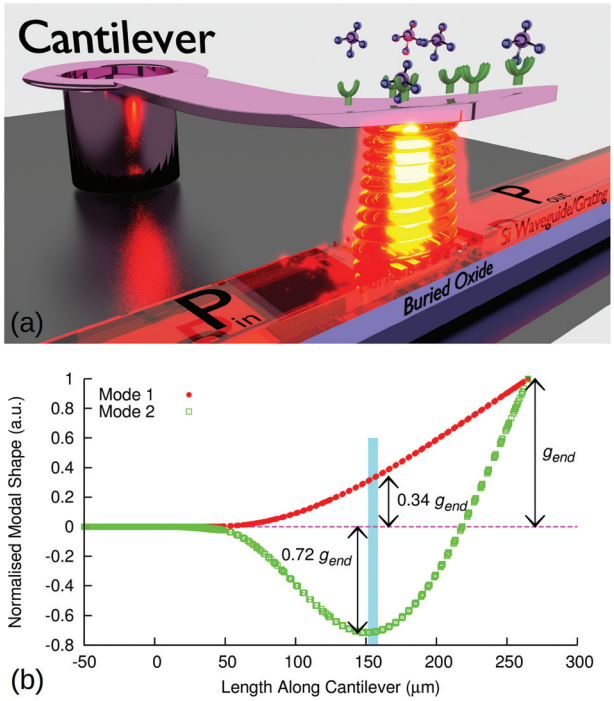

Fig. 1 (a) Isometric image of cantilever position sensing structure (not to scale). (b) Modeled normalized modal shapes of the cantilever for the first two vibration modes (normalization is to the end deflection for each mode, g_{end}). The highlighted area represents the measured cantilever region over the diffraction grating. The outer circumference of the top-hat anchor starts at −50 μm and ends at +50 μm along the *x*-axis, which is the starting point of the suspended beam.

package,[25] and then fabricated by the Laboratoire d'électronique et de technologie de l'information (LETI) *via* the ePIXfab program on a silicon on insulator (SOI) wafer using their standard passive process.[26] The buried oxide (BOX) layer of the wafer was 2 μm thick, under a 220 nm thick epitaxial silicon layer. The waveguides and square wave gratings (pitch 630 nm, depth 70 nm) were etched into the epitaxial silicon using deep ultra-violet (DUV) lithography. Subsequently, silicon dioxide was deposited to cover the structures and planarized using chemo-mechanical polishing (CMP) down to a thickness of 100 nm above the waveguides.

The grating couplers were designed to be broadband and have optimized coupling efficiency for light at the wavelength of 1550 nm. The gratings are built to the same dimensions and specifications as the uniform grating in SOI with oxide top cladding analysed by Taillaert *et al.*[27]

The cantilevers were fabricated on the planarized sample surface as received from LETI at The University of Western Australia. Low stress HD MicroSystems PI-2610 polyimide of thickness 1.6 μm was used as the sacrificial layer. Plasma enhanced chemical vapour deposition (PECVD) silicon nitride was used as the structural material for cantilevers with a 3/50 nm thick thermally evaporated chromium/gold undercoat to achieve high reflectivity at infra-red wavelengths[28] with the chromium layer used as a stiction layer to the SiN_x. The

cantilever beams used were 200 μm long, 20 μm wide, and 750 nm thick, with top hat style anchors down to the SiO_2 chip surface layer. Thermally evaporated gold was used for bottom electrostatic actuation pads and wiring, and the cantilever gold undercoat layer served as the cantilever top actuation electrode.

The cantilever was designed and modelled using finite element method (FEM) analysis *via* the Coventorware software package. This nonlinear modal FEM analysis was performed using Coventorware's proprietary implementation of the Lanczos iteration method[29] to obtain the frequencies and shapes of the first two mechanical modes of the cantilever. The cantilever dimensions modelled are as stated above for the fabrication process. The silicon nitride layer was modelled as a dielectric solid with Young's modulus of 220 GPa, Poisson's ratio of 0.27, and a density of 2700 kg m^{-3}. The gold undercoat layer was modelled as a conductive solid with Young's modulus of 57 GPa, Poisson's ratio of 0.35, and a density of 19 300 kg m^{-3}. The volume mesh used for both layers was a 10 node parabolic tetrahedral mesh. The modelled beam shapes for the first two vibrational modes are shown in Fig. 1(b), with the region above the grating highlighted as the blue shaded area. The modelling predicted that when the cantilever is excited at its resonance frequency (Mode 1), the region measured by the grating will move by 34% of the cantilever tip motion amplitude, whereas when excited at its first harmonic frequency (Mode 2), the region measured by the grating will move by 71% of the cantilever tip amplitude. All cantilever position and movement measurements quoted in this work are made in the region above the grating unless otherwise specified.

Cantilever electrostatic actuation was controlled by an Agilent 33220A arbitrary waveform generator. A Polytec OFV-5000 vibrometer controller with a DD-500 displacement decoder and an OFV-552 differential fiber sensor head was used to monitor the displacement of the cantilever and to measure the mechanical resonance frequency. A Zygo NewView 7300 optical profilometer was used to measure the initial shape and state of the cantilever.

Laser light was launched into and out of the on-chip silicon photonic waveguides *via* SMF-28 optic fiber that was aligned to out-of-plane grating couplers integrated into the waveguides. All measurements were performed in an open atmosphere in ambient room temperature and pressure conditions.

4. Results and analysis

A scanning electron microscope (SEM) image of the tested cantilever is shown in Fig. 2. It can be seen that the cantilever is not perfectly flat, but rather curves up from the anchor to the tip due to residual stresses. Using the Zygo NV 7300 system, optical profilometry confirmed that at rest, the middle and the tip of the beam were 4.5 μm and 11.5 μm higher than the start of the beam near the anchor.

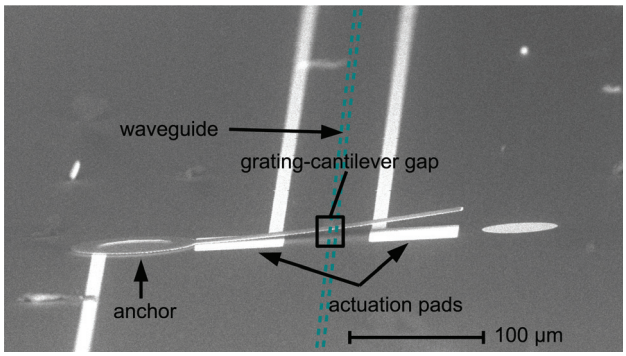

Fig. 2 SEM image of the tested cantilever. Electrostatic pads are used to actuate the cantilever. The track on the bottom left of the image provides electrical contact to the top electrode running along the bottom of the suspended cantilever beam. The tracks running from the top of the image are electrically connected to each other, and provide electrical contact to the two bottom actuation pads. The optical waveguide with the diffraction grating (not visible) are embedded below a SiO_2 planarization layer and run perpendicularly underneath the middle of the cantilever beam as indicated by the dashed line on the image. Note that due to fabrication stresses, the cantilever tip's rest position is visibly higher than the anchor platform.

The cantilever was electrostatically actuated at its resonant frequency of 13.2 kHz (Mode 1), as measured using a commercial vibrometer, and the light transmitted through the waveguide measured on an InGaAs photodiode through the SMF-28 optic fibre. The detected signal for a wavelength of 1550 nm is plotted as a function of grating-cantilever gap over a range from 4.3–6.5 μm in Fig. 3(a), and a strong amplitude modulation due to gap change is evident. As this modulation effect is interferometric in nature, the amplitude does not monotonically increase, but is periodic with respect to the gap size. Fig. 3(a) includes an overlay of a 2-D FDTD simulation of the expected outputs of the structure. The model was based on the fabricated SOI platform for the optical waveguide/grating structure, which consisted of a 220 nm epitaxial silicon layer for the waveguide, 2000 nm thick buried oxide for the bottom cladding layer, and a silicon handle wafer as the base. The grating is a square-wave grating of 610 nm pitch, 70 nm depth and 11.9 μm length. In this model, the bottom surface of the suspended cantilever is assumed to be a perfect reflector at the wavelength of interest (1550 nm), and extending 1 μm beyond the interrogating grating on all sides. For the power calculations of this model, a TE polarized Gaussian beam at a wavelength of 1550 nm was launched into the waveguide. The diffraction grating was placed a sufficient distance away (8 μm) from the source so that a stable optical mode was incident on the grating section of the waveguide. The FDTD simulations were run for various values of cantilever to grating separation in the range from 4 to 7 μm. The power calculations from the simulation data were performed over the cross section of the waveguide with the power in the substrate modes and small evanescent fields not included in the power summations. The simulation methodology used here has been previously provided in greater detail by the authors.[30]

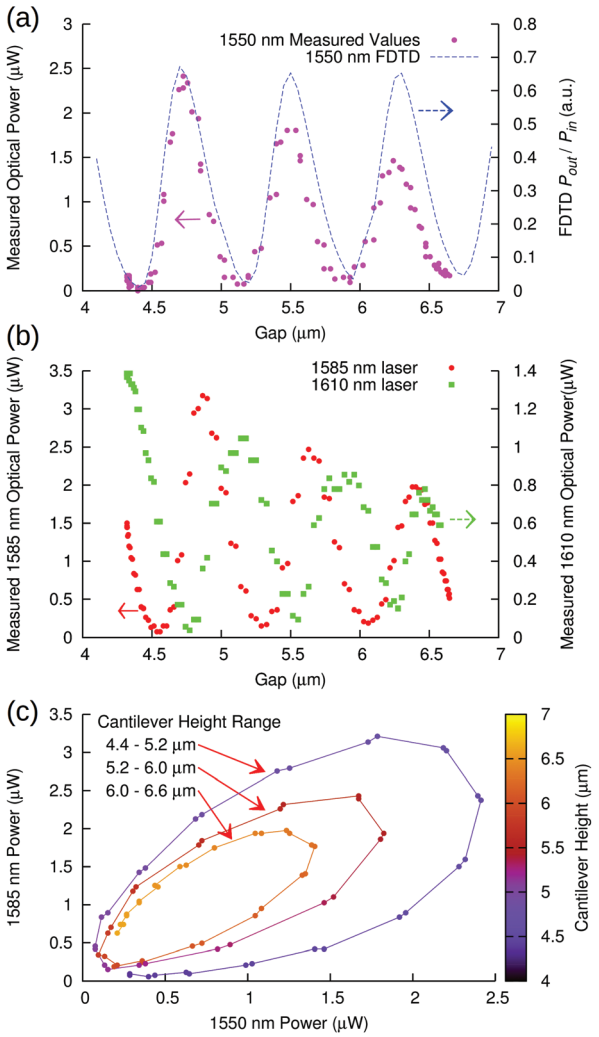

Fig. 3 (a) Measured and FDTD simulated optical output of the device for 1550 nm transmitted light as a function of cantilever-grating gap. (b) Measured optical output of the device *vs.* cantilever-grating gap for 1585 and 1610 nm transmitted light. Differing *y*-axis scales are used here due to the experimental setup having different coupling efficiencies into the chip for the various laser wavelengths tested. (c) Locus of points obtained by comparing measured 1550 and 1585 nm wavelength output power for matching cantilever positions as the cantilever beam travels through its movement range. Each arm of the spiral represents approximately an 800 nm segment of cantilever travel as indicated by the colour scale.

The measured results show good correlation to the simulation data, however, it can be seen in Fig. 3(a) that in comparison to the simulation data the peak amplitude of each cycle of the measured data decreases by a successively larger amount for successively increasing gap size. This can be mainly attributed to the fact that the 2-D simulations did not take into account the deflection angle of the cantilever as it moves, and so do not consider light lost by reflection away from the grating. 3-D FDTD simulations are able to account for this effect, but are far more memory- and computationally-expensive to generate, and so were not performed for the scope of this work.

4.1 Multiple wavelengths

In addition to measurements of light transmitted at a wavelength of 1550 nm for which the performance of the diffraction gratings was maximised, we undertook measurements using both 1585-, and 1610 nm wavelength lasers. The corresponding results are shown in Fig. 3(b). The periodic nature of the interferometric output is strongly maintained over this 60 nm wavelength range. In addition, FDTD simulations (not shown) suggest that this interferometric effect is maintained over a broader wavelength range of ±100 nm. This wide range of operation is compatible with implementation of an on-chip wavelength division multiplexing (WDM) system to read-out the movement of multiple cantilevers in a scheme where each row of cantilevers is addressed with a different wavelength.[23] As optical interferometric techniques are not monotonic, the cantilever position read-out can be ambiguous if the range of movement is greater than the periodicity of the output signal. This ambiguity could potentially cause problems for device concepts requiring position measurements over a large dynamic range. To demonstrate that this problem can be mitigated using multiple wavelengths, we show in Fig. 3(c) the locus of points obtained when the 1550 and 1585 nm wavelength output signals for the same cantilever position are plotted against each other. This figure shows that the locus follows a spiral, and so using only two wavelengths, the positional ambiguity can be resolved for most positions over a dynamic range of 3 μm, for gap distance between 4 and 7 μm as indicated by the colour scale in Fig. 3(c). The position of the cantilever for the low optical powers (bottom left corner of Fig. 3(c)) may be difficult to discern. This could be solved by either improving the signal to noise ratio through the use of higher powered input lasers (or more efficient input/output coupling), by choosing laser wavelengths that do not approach power throughput local minima for similar cantilever-grating separations, or by adding a third laser wavelength such as the 1610 nm laser from Fig. 3(b).

The results from Fig. 3(a) show that in the quasi-linear region over the range from 4.5–4.7 μm, the optical power increases by 2.1 μW (approx. 10 dB). The slope of the curve in this region is proportional to the sensitivity and is determined to be 10 nW nm^{-1}.

4.2 Frequency sweep

To investigate the dynamic mode operation, we performed electrostatic sine wave actuation of the cantilever. In this experiment, the optical output of the waveguide was detected by an InGaAs photodetector which was connected to a Stanford Research Systems SR830 lock-in amplifier. The cantilever was then actuated by a sine wave with a peak-to-peak voltage of 10 mV for a frequency sweep between 1 kHz and 100 kHz in increments of 100 Hz. The time constant of the lock-in amplifier was set to 100 ms, and the measured transmitted optical power density is shown in Fig. 4 as a function of actuation frequency. These measurements show two frequency peaks. The main peak is found at 13.2 kHz (f_0) and

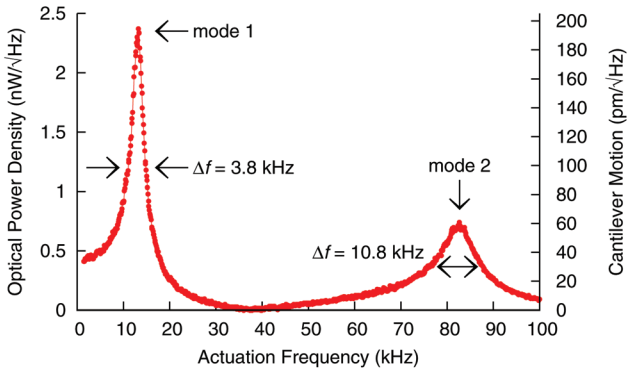

Fig. 4 Measured optical signal transmitted through the presented read-out technique as a function of cantilever actuation frequency when the cantilever is subjected to a frequency sweep from 1 to 100 kHz using sine wave actuation with a peak to peak voltage of 10 mV.

corresponds to the cantilever resonant frequency, matching the value measured using a commercial vibrometer. The second peak corresponding to the first harmonic frequency is seen at 82.7 kHz (f_1), with the ratio between the resonance frequency and the first harmonic frequency 82.7/13.2 = 6.27. The harmonic frequencies of a cantilever can be found from the solutions to the frequency equation for a cantilever beam[31] and it can be shown that the ratio of the frequencies of mode 2 to mode 1 (f_1/f_0) for a cantilever with rectangular cross-section is equal to 6.27, matching our measurements.

4.3 Step response

The resonant frequency of the cantilever can also be measured by applying a small step actuating voltage to the beam, and subsequently monitoring the transmitted signal. This capability is especially useful for sensing using the dynamic mode where a simple test for resonance frequency of the cantilever is required. This time domain step response for our cantilever is shown in Fig. 5, where we observe a typical second order step response for an underdamped cantilever beam with step induced oscillations at the resonant frequency exponentially decaying in magnitude due to damping. We can fit the measured step response results presented in Fig. 5 to an equation representing the second order step response of an underdamped system, $z(t)$, as a function of time, t,

$$z(t) = A\left[1 - \frac{1}{\sqrt{1-\zeta^2}} e^{-\zeta 2\pi f_0 t} \cos\left(2\pi f_0 \sqrt{1-\zeta^2} t\right)\right] + C \quad (1)$$

where A is a scaling constant representing the combined optical response to the cantilever mechanical response to the electrostatic step voltage, and C is the final settling amplitude. Using the presented data and the logarithmic decrement technique,[31] we calculate the damping ratio (ζ) to be 0.07, and the natural frequency of the system (f_0) to be 13.2 kHz – again matching the previous resonant frequency measurements. From the determined damping ratio, we calculate the quality factor of the beam to be $Q = 1/2\zeta = 7.2$, which is used in our subsequent Brownian motion calculations. The ability to determine the resonant frequency of the cantilever using on-chip compatible low voltage step actuation is highly attractive for dynamic mode cantilever sensors.

4.4 Brownian stimulated motion

To test the experimental detection limits of the presented read-out system, the actuation signal to the cantilever was disconnected, and we attempted to detect movement of the cantilever due to room temperature stimulated thermal Brownian motion. Measurements for the Brownian motion were conducted by connecting the signal from the optical output grating directly to an Agilent ESA-E Series model E4402B spectrum analyzer. These measurements were made using a resolution bandwidth (RBW) of 1 kHz. As the measurements were performed in an open environment, we expected some additional acoustic noise from the laboratory environment to also affect the cantilever. Fig. 6 presents the measured optical power transmitted through the read-out device under the described room ambient conditions. This measurement shows the same two peaks at 13.2 kHz and 82.7 kHz as observed in Fig. 4 in response to an electrostatic actuation frequency sweep at 10 mV, however, in this measurement, these peaks are entirely due to environmentally stimulated motion. A noise

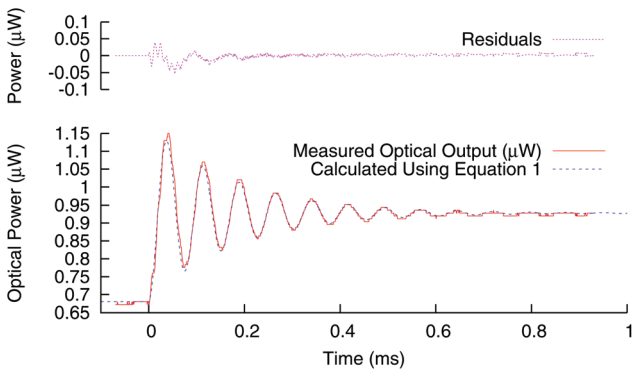

Fig. 5 Measured optical response of the presented read-out technique to an actuation step voltage of 5 V at time t = 0 ms.

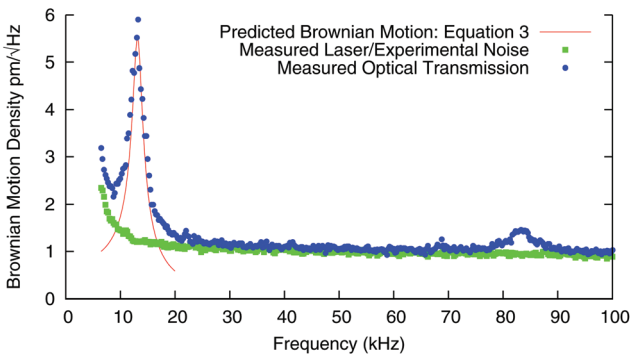

Fig. 6 Measured optical power modulation of the read-out device compared to the predicted Brownian noise envelope for the cantilever. Measurement of the noise of the laser when coupled through the chip without an overlying cantilever is also presented.

floor of 1 pm per $(\mathrm{Hz})^{-1/2}$ is seen. Accordingly, since the RBW of the spectrum analyser used was 1 kHz, this corresponds to cantilever minimum detectable deflection (MDD) of $1\,\mathrm{pm\,per}\sqrt{\mathrm{Hz}} \times \sqrt{1\,\mathrm{kHz}} = 32\,\mathrm{pm}$. Above that noise floor, sub-pm per $(\mathrm{Hz})^{-1/2}$ resolution is clearly observed. The smaller peak at 82.7 kHz can be clearly resolved at 0.3 pm per $(\mathrm{Hz})^{-1/2}$ above the noise floor – corresponding to an deflection of $0.3\,\mathrm{pm\,per}\sqrt{\mathrm{Hz}} \times \sqrt{1\,\mathrm{kHz}} = 9.5\,\mathrm{pm}$ when above the noise floor. This is an exceptional result.

A measurement of the laser power coupled into and back out of the silicon photonic waveguide on the sample chip without an overlying cantilever was also performed, and is included in Fig. 6 as a function of vibrational frequency. This provides a combined measurement of the noise arising from relative intensity noise (RIN), shot noise and fiber input/output (I/O) vibration induced noise. The RIN in this system could be reduced by the use of a low RIN laser, or *via* other RIN compensation techniques.[32] Shot noise can be decreased through the use of either a higher power laser, or better coupling into and out of the chip. Fiber I/O vibrational noise could be removed completely by mounting laser diodes and photodiodes directly onto the chip. The noise due to all these components in our equipment can be seen in Fig. 6 to be around 1 pm per $(\mathrm{Hz})^{-1/2}$, matching the noise floor as observed when the same laser is transmitted through a waveguide with an overlying cantilever.

Due to interest in characterizing cantilevers for use in AFMs, substantial work in the literature has been performed on the topic of predicting Brownian motion for a cantilever. The vertical z-direction component of the Brownian noise density, $n_{\mathrm{zb}}(f)$, of a cantilever tip around its resonant frequency can be predicted by[33]:

$$n_{\mathrm{zb}}(f) = \sqrt{\frac{2k_{\mathrm{b}}T}{\pi Q k f_0}\frac{1}{\left(1-\left[\left(\frac{f}{f_0}\right)^2+\frac{f}{f_0 Q}\right]^2\right)}} \qquad (2)$$

where k_{b} is Boltzmann's constant, T is temperature (K), Q is the quality factor of the cantilever, k is the spring constant of the cantilever, f_0 is the resonant mechanical frequency of the cantilever, and f is the frequency of interest. Note that this equation does not model Brownian motion around higher mechanical modes of the cantilever. For our cantilever, Q = 7.2, f_0 = 13.2 kHz, T = 293 K, and k = 6.06 mN m^{-1} (calculated using Sader *et al.*[34]).

From Fig. 1(b), we know that at frequencies near the fundamental, the region measured by our grating will only move 34% the distance that the tip moves, so the Brownian noise density at the midpoint above the interrogating grating, $n_{\mathrm{zbm}}(f)$, can be estimated simply by:

$$n_{\mathrm{zbm}}(f) = 0.34 n_{\mathrm{zb}}(f) \qquad (3)$$

This function is plotted in Fig. 6 for our cantilever using the solid line. It can be seen that around the resonance frequency the measured values follow the envelope predicted by eqn (3) extremely well. This gives the confidence that the motion of the cantilever is stimulated mostly thermally rather than *via* other mechanisms such as acoustic noise of the laboratory environment. The presented results show that the investigated read-out technique is sufficiently sensitive to detect Brownian motion of the cantilever beam in common room ambient conditions and that the cantilever beam can be well characterized in terms of the expected mechanical performance.

It is envisaged that it will be important for the presented read-out technique to operate in fluid environments, especially for applications in the biological and medical domain. Due to the mechanical damping that is experienced by cantilevers in viscous media, higher Q cantilevers than those that were fabricated for this work will be required. The interrogating grating at the core of the measurement system will also have to be slightly redesigned for optimal optical performance in media with refractive indices higher than air. For the specific case of aqueous media, water strongly absorbs infrared radiation, and so there will be additional optical power losses when using this read-out technique in aqueous environments. Depending on the cantilever-grating separation and the finesse of the cavity, the optical path length travelled by the light could be over one hundred microns, and 1550 nm light has a transmittance of 0.5 through 1 mm of water.[35] There may also be some scattering losses due to the inhomogeneity of some fluid media, *e.g.* small particulates suspended in water. Any inhomogeneities in the optical properties of the media surrounding the cantilever, and in particular their dynamic changes will influence the optical propagation measurement. These combined issues may have the effect of limiting fluid-based applications of this technology to media with low opacity for the transmitted wavelength and low turbidity.[12]

5. Conclusions

We have demonstrated an integrated on-chip approach for measuring mechanical motion on the picometer scale over a dynamic range of several microns. We show that the technique is sufficiently sensitive to detect cantilever movement due to Brownian motion stimulated and measured in open ambient room temperature and pressure. Cantilevers are fabricated above silicon photonic structures manufactured using standard CMOS processing. Combined with the measurement sensitivity makes this technique attractive for applications requiring discovery of on chip microscale motion, including monitoring of mechanical resonant frequency. In addition, the demonstrated on-chip approach is scalable to addressing large arrays of cantilevers on a single chip.

These characteristics are highly desirable for example for AFM applications as well as on-chip MEMS-based chemical/biological sensors and on-chip integrated force or pressure sensors operating at picometer scale sensitivities. An important achievement of the technique is its ability to maintain this sensitivity in common ambient conditions, allowing for a transition of the emerging MEMS-based sensing technologies

to be taken from laboratory controlled environments into real world conditions enabling many new applications.

Acknowledgements

This work has been supported by the Commonwealth of Australia under the Australia-India Strategic Research Fund under ST030019, the Australian Research Council, and the Australian National Fabrication Facility – Western Australia node.

References

1 Y. T. Yang, C. Callegari, X. L. Feng, K. L. Ekinci and M. L. Roukes, *Nano Lett.*, 2006, **6**, 583–586.
2 M. Li, H. X. Tang and M. L. Roukes, *Nat. Nanotechnol.*, 2007, **2**, 114–120.
3 F. Huber, H. P. Lang, N. Backmann, D. Rimoldi and C. Gerber, *Nat. Nanotechnol.*, 2013, **8**, 125–129.
4 G. Wu, R. H. Datar, K. M. Hansen, T. Thundat, R. J. Cote and A. Majumdar, *Nat. Biotechnol.*, 2001, **19**, 856–860.
5 T. P. Burg, M. Godin, S. M. Knudsen, W. Shen, G. Carlson, J. S. Foster, K. Babcock and S. R. Manalis, *Nature*, 2007, **446**, 1066–1069.
6 Y. F. Dufrêne, *Nat. Rev. Microbiol.*, 2008, **6**, 674–680.
7 S. E. Cross, Y.-S. Jin, J. Rao and J. K. Gimzewski, *Nat. Nanotechnol.*, 2007, **2**, 780–783.
8 G. Longo, L. Alonso-Sarduy, L. M. Rio, A. Bizzini, A. Trampuz, J. Notz, G. Dietler and S. Kasas, *Nat. Nanotechnol.*, 2013, **8**, 522–526.
9 Y.-E. Choi, J.-W. Kwak and J. W. Park, *Sensors*, 2010, **10**, 428–455.
10 J. W. Ndieyira, N. Kappeler, S. Logan, M. A. Cooper, C. Abell, R. A. McKendry and G. Aeppli, *Nat. Nanotechnol.*, 2014, **9**, 225–232.
11 F. Huber, H. P. Lang and C. Gerber, *Nat. Nanotechnol.*, 2014, **9**, 165–167.
12 N. V. Lavrik, M. J. Sepaniak and P. G. Datskos, *Rev. Sci. Instrum.*, 2004, **75**, 2229–2253.
13 A. Loui, T. V. Ratto, T. S. Wilson, S. K. McCall, E. V. Mukerjee, A. H. Love and B. R. Hart, *Analyst*, 2008, **133**, 608.
14 M. K. Baller, H. P. Lang, J. Fritz, C. Gerber, J. K. Gimzewski, U. Drechsler, H. Rothuizen, M. Despont, P. Vettiger and F. M. Battiston, *Ultramicroscopy*, 2000, **82**, 19.
15 G. S. Shekhawat and V. P. Dravid, *Nat. Nanotechnol.*, 2013, **8**, 77–78.
16 T. H. Stievater, W. S. Rabinovich, M. S. Ferraro, J. B. Boos, N. A. Papanicolaou, J. L. Stepnowski and R. A. McGill, Proceedings of SPIE, San Jose, CA, USA, 2007, pp. 64640D–64640D–10.
17 D. Kong, T. Mei, Y. Tao, L. Ni, T. Zhang, W. Lu, Z. Zhang and R. Wang, *Information Acquisition, 2004*, Proceedings. International Conference on, 2004, p. 278281.
18 G. Binnig, M. Despont, U. Drechsler, W. HÃberle, M. Lutwyche, P. Vettiger, H. J. Mamin, B. W. Chui and T. W. Kenny, *Appl. Phys. Lett.*, 1999, **74**, 1329–1331.
19 C. Schonenberger and S. F. Alvarado, *Rev. Sci. Instrum.*, 1989, **60**, 31313134.
20 K. Zinoviev, C. Dominguez, J. A. Plaza, V. J. C. Busto and L. M. Lechuga, *J. Lightwave Technol.*, 2006, **24**, 2132.
21 J. W. Noh, R. Anderson, S. Kim, J. Cardenas and G. P. Nordin, *Opt. Express*, 2008, **16**, 12114–12123.
22 T. H. Stievater, W. S. Rabinovich, M. S. Ferraro, N. A. Papanicolaou, R. Bass, J. B. Boos, J. L. Stepnowski and R. A. McGill, *Opt. Express*, 2008, **16**, 2423–2430.
23 G. Putrino, A. Keating, M. Martyniuk, L. Faraone and J. Dell, *IEEE Photonics Technol. Lett.*, 2012, **24**, 2243–2246.
24 X. Li and D.-W. Lee, *Meas. Sci. Technol.*, 2012, **23**, 022001.
25 A. F. Oskooi, D. Roundy, M. Ibanescu, P. Bermel, J. Joannopoulos and S. G. Johnson, *Comput. Phys. Commun.*, 2010, **181**, 687–702.
26 P. Dumon, W. Bogaerts, R. Baets, J.-M. Fedeli and L. Fulbert, *Electron. Lett.*, 2009, **45**, 581–582.
27 D. Taillaert, F. Van Laere, M. Ayre, W. Bogaerts, D. Van Thourhout, P. Bienstman and R. Baets, *Jpn. J. Appl. Phys.*, 2006, **45**, 6071–6077.
28 J. M. Bennett and E. J. Ashley, *Appl. Opt.*, 1965, **4**, 221–224.
29 C. Lanczos, *An iteration method for the solution of the eigenvalue problem of linear differential and integral operators*, United States Governm. Press Office, 1950.
30 G. Putrino, A. Keating, M. Martyniuk, L. Faraone and J. Dell, *J. Lightwave Technol.*, 2012, **30**, 1863–1868.
31 W. W. Jr, S. P. Timoshenko and D. H. Young, *Vibration Problems in Engineering*, John Wiley & Sons, 1990.
32 L. Fock, A. Kwan and R. Tucker, *J. Lightwave Technol.*, 1992, **10**, 1919–1925.
33 T. Fukuma, M. Kimura, K. Kobayashi, K. Matsushige and H. Yamada, *Rev. Sci. Instrum.*, 2005, **76**, 053704.
34 J. E. Sader, J. W. M. Chon and P. Mulvaney, *Rev. Sci. Instrum.*, 1999, **70**, 3967–3969.
35 H. Döscher, J. F. Geisz, T. G. Deutsch and J. A. Turner, *Energy Environ. Sci.*, 2014, **7**, 2951–2956.